Sensors & Actuators: B. Chemical 329 (2021) 129131

Contents lists available at ScienceDirect

Sensors and Actuators: B. Chemical

journal homepage: www.elsevier.com/locate/snb

Soft-lithographically line-patterned In-doped ZnO quantum dots with hydrothermally grown ZnO nanocolumns for acetone detection

Jun Ho Lee [1], Seung-Eun Baek [1], Hyun-Sook Lee, Dahl-Young Khang *, Wooyoung Lee *

Department of Materials Science and Engineering, Yonsei University, 50 Yonsei-ro, Seodaemun-gu, Seoul, 03722, Republic of Korea

ARTICLE INFO

Keywords:
Gas sensors
Metal oxide semiconductors
In-doped ZnO quantum dots
Acetone

ABSTRACT

We introduced a new approach to enhance the sensing performance of sensors based on metal oxide semiconductors. We synthesized In-doped ZnO quantum dots (IZO QDs) by a hydrothermal method and fabricated line-patterned IZO QD layers with polydimethylsiloxane (PDMS) molds. Additional hydrothermal growth was conducted to create ZnO nanocolumns (NCs) on the patterned surfaces. Thus, drop-cast and line-patterned sensors and line-patterned samples with NCs grown for 0.5 h (NC(0.5 h)/Line) and 4 h (NC(4 h)/Line) were prepared. Among these four different sensors, the NC(0.5 h)/Line sensor exhibited an excellent response of 26,000 with fast response times of less than 1 s to 10 ppm of acetone. In addition, the detection limit was approximately 0.1 ppm of acetone, and the resistance was almost constant even after repeatability tests. According to UV–vis and X-ray photoelectron spectroscopic analyses, the extraordinary sensing characteristics of NC(0.5 h)/Line were mainly because this sensor had the largest optical band energy and the highest ratio of oxygen vacancies among the tested sensors. On the other hand, the NC(4 h)/Line sensor showed the lowest response of the four sensors. During the long-term growth of NCs, —OH groups are produced on the surface of the material, and $Zn(OH)_2$ NCs are formed instead of ZnO NCs, resulting in a large decrease in the carrier concentration and active sites. In conclusion, we developed highly sensitive acetone sensors by constructing special morphologies.

1. Introduction

The detection of biomarkers for some diseases via exhaled breath is a promising diagnostic method without invasive blood sampling. The concept of breath analysis for disease diagnosis was first proposed by Hippocrates in ancient Greece, who claimed that aromas in human breath could provide diagnostic information [1,2]. In 1970, after Lavoisier proved the presence of CO_2 in exhaled breath in the 18th century, Pauling demonstrated that human breath is a mixture of over 200 different kinds of volatile organic compounds (VOCs), such as H_2, CO_2, acetone, and methane. Recently, over 1000 gases have been determined in human breath, and some endogenously produced VOCs provide valuable information about metabolism [3]. Since people with certain diseases show altered metabolic pathways, their exhaled breath composition may exhibit some variations [4,5]. For example, patients with diabetes could have higher concentrations of acetone and isoprene, and those with asthma could have higher concentrations of acetone, nitric oxide and ethane. Consequently, exhaled breath analysis technology can be a new option for disease diagnosis.

In particular, analysis of acetone in breath is necessary due to its role as a biomarker for diabetes, which is a common disease. Acetone is mainly produced by fat metabolism inside the liver. The acetone concentration is approximately 1 ppm for normal individuals and over 10 ppm for diabetic individuals. During fat metabolism, in a cycle in which acetoacetyl-CoA is converted to acetyl-CoA via β-hydroxy-β-methylglutaryl-CoA, acetoacetate is produced as a byproduct, and acetone is later derived by decarboxylation [4,5]. Therefore, the concentration of acetone in exhaled breath may be attributed to a higher rate of fat metabolism, and highly sensitive gas sensors for the detection of acetone are necessary.

Various materials have been investigated as candidates for acetone gas sensors. In particular, many studies have focused on metal oxide semiconductors such as ZnO [6–11], SnO_2 [12–14] and WO_3 [15,16]. Among them, ZnO is considered an appropriate sensing material due to its high band gap, high sensitivity, and various nanostructures. Sensors fabricated with various nanostructures using ZnO might have improved

* Corresponding authors.
E-mail addresses: dykhang@yonsei.ac.kr (D.-Y. Khang), wooyoung@yonsei.ac.kr (W. Lee).
[1] These authors contributed equally.

https://doi.org/10.1016/j.snb.2020.129131
Received 25 June 2020; Received in revised form 14 October 2020; Accepted 26 October 2020
Available online 31 October 2020

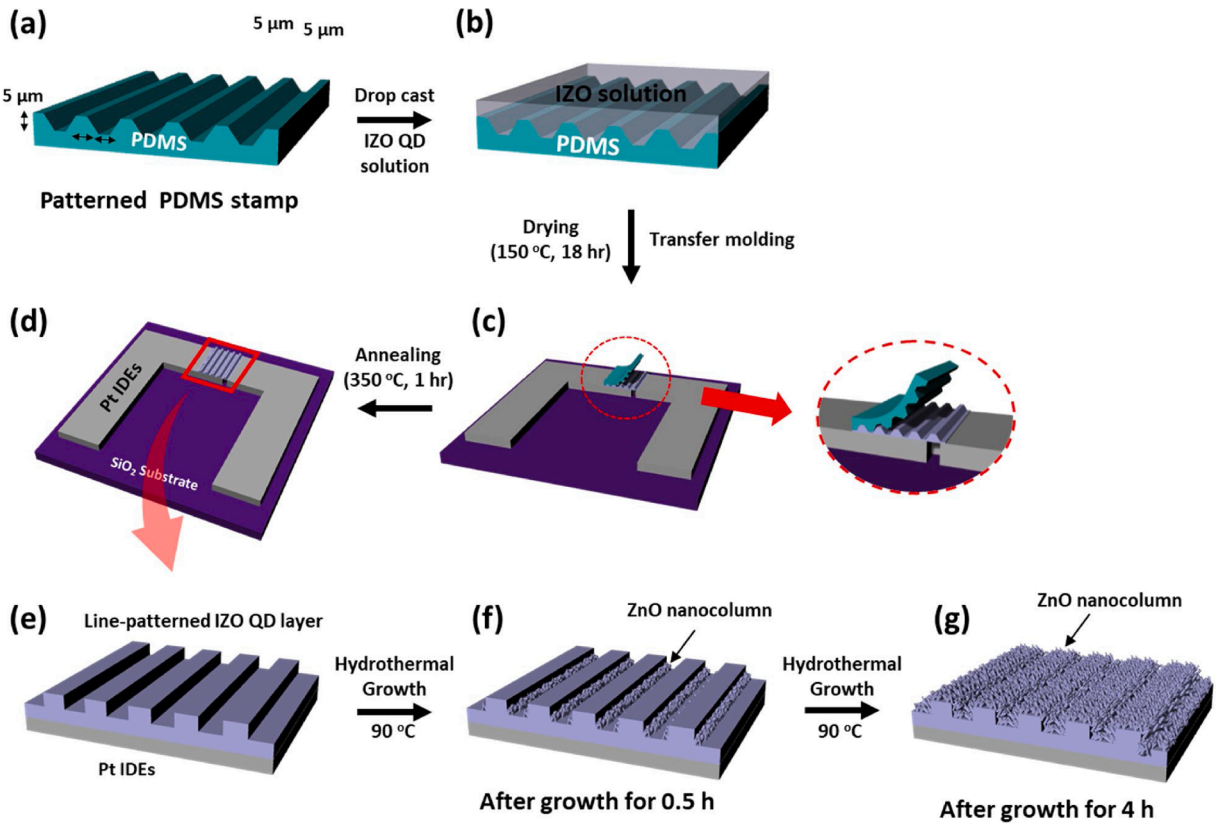

Fig. 1. Schematic illustration of fabrication process for various gas sensors by transfer molding technique. The line-patterned samples can further be grown with ZnO NC by hydrothermal method. (a) Geometry of PDMS stamp, with (b) drop-cast IZO QD dispersion. After micro-transfer molding onto sensor substrate with IDE ((c), (d)), various sensors are fabricated as (e) the line-patterned, (f) line-patterned with 0.5 h growth and (g) line-patterned with 4 h growth of ZnO NC.

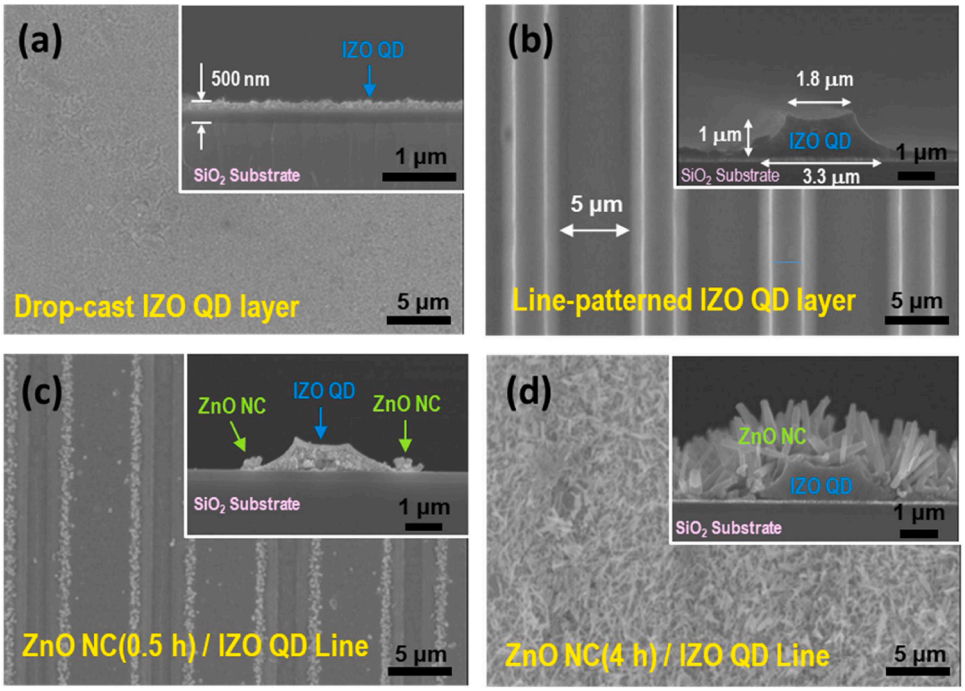

Fig. 2. SEM images of (a) drop cast IZO QD layer, (b) line-patterned IZO QD layer, (c) ZnO NC(0.5 h)/IZO QD line and (d) ZnO NC(4 h)/IZO QD line samples (top view, scale bars =5 μm). Insets depicted side views of respective sensors (scale bars =1 μm).

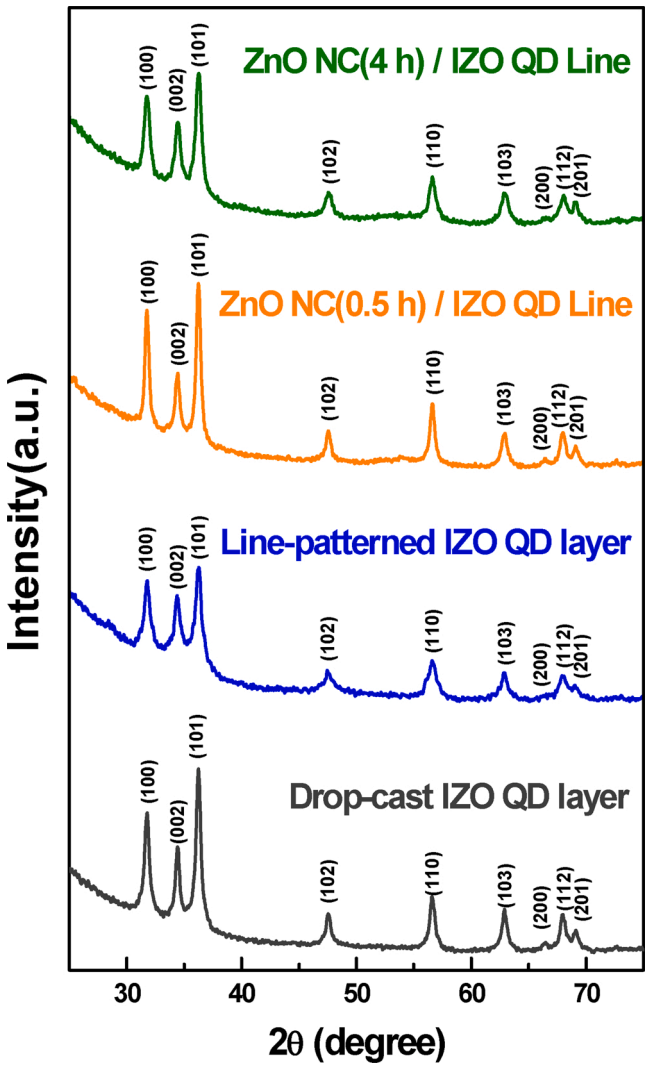

Fig. 3. XRD results of drop cast IZO QD layer (black), line patterned IZO QD layer (red), ZnO NC(0.5 h)/IZO QD line (orange), and ZnO NC(4 h)/IZO QD line (green), respectively. (For interpretation of the references to colour in this figure legend, the reader is referred to the web version of this article).

sensing properties due to the increased number of active sites for target gas molecules [17]. ZnO sensing was conducted by the reaction of oxygen ions adsorbed on the ZnO surface with the target gas molecules. When ZnO is exposed to atmospheric air, the oxygen molecules in air are adsorbed on the ZnO surface and capture the electrons from the conduction band of ZnO, producing adsorbed oxygen species. This leads to the formation of an electron depletion layer on the ZnO surface, which increases the electrical resistance in ZnO. When ZnO is exposed to the target gas, the electrons released via a sensing reaction return to the conduction band of ZnO. This leads to a reduction in the thickness of the electron depletion layer, resulting in reduced electrical resistance of ZnO. Therefore, the sensing performance is highly dependent on the thickness of the depletion layer (amount of adsorbed oxygen ions or reactive sites). Accordingly, nanostructured ZnO with high surface area and large depletion layer can afford large change in resistance when exposed to the target gas [17].

Recently, sensors based on ZnO quantum dots (QDs) were reported to be highly sensitive when sensing various gases, such as acetone [6], isoprene [7], and 2-chloroethyl ethyl sulfide (2-CEES) [8], by reducing the size of particles and doping with Al. Additionally, doping of In into ZnO QDs was investigated for the detection of acetylene, and it showed much better sensing performance than pure ZnO QDs and ZnO QDs doped with other elements [9]. In general, the metal dopants increase the activity as well as modify the particle size [17]. The improved sensing performance of In-doped ZnO QDs (IZO QDs) was attributed to the increased surface area, which was a result of the decrease in particle size induced by In doping [9]. The larger ion radius of In^{3+} induced a higher compressive stress in the crystal structure [18], thus forming IZO QDs with a smaller crystallite size. Therefore, we speculated that IZO QDs would also show enhanced sensing properties for acetone; however, these ZnO-QD-based sensors were prepared only in film forms by drop casting. Therefore, we decided to develop gas sensors with patterned nanostructures based on IZO QDs to have a large surface area or a large sensing area.

To fabricate materials in new morphologies with large surface areas, we adopted the soft lithography technology. Soft lithography is a non-photolithography method that is based on self-assembly and replica molding for microfabrication [19,20]. The process can be advantageous in terms of fast prototyping capabilities and simple production without expensive equipment. In particular, soft lithography is expected to create uniquely patterned microstructures based on IZO QDs through microtransfer molding, which is one of the soft lithography methods utilized to fabricate interconnected and isolated microstructures for organic polymers [19]. The patterned IZO QD nanostructures are, thus, expected to exhibit improved sensing performance compared with drop-casted IZO QD film. To increase the number of active sites for sensing, the patterned IZO QD surfaces were decorated with ZnO NCs.

In this paper, we report on the effect of morphologies on the sensing performance by fabricating a patterned IZO film for acetone detection. IZO QDs were synthesized by a hydrothermal method and reconstructed into line patterns by soft lithography. Further growth of ZnO on the surface was conducted by hydrothermal growth. Through these methods, we were able to improve the sensing properties of acetone from drop-cast samples. In particular, optimized sensors exhibited extremely high sensitivity and selectivity towards acetone. The results were analyzed by comparing the optical band gap and oxygen vacancies via UV–vis spectroscopy and X-ray photoelectron spectroscopy (XPS), respectively.

2. Materials and methods

2.1. Synthesis of In-doped ZnO (IZO) QDs

IZO QDs were synthesized by a hydrothermal method. First, zinc acetate dehydrate (0.1 M, $Zn(CH_3COO)_2{\cdot}2H_2O$, Alfa Aesar) and indium chloride ($InCl_3$, 1 at%, Sigma-Aldrich) were dissolved in *N,N*-dimethylmethanamide (DMF, C_3H_7NO) to prepare a zinc precursor solution. Then, tetramethylammonium hydroxide solution (TMAH, $(CH_3)_4NOH{\cdot}5H_2O$, 0.3 M, Sigma-Aldrich) was mixed with methanol. The zinc precursor solution was slowly dropped into the TMAH solution, and the mixture was stirred at 30 °C for 1 h. The resulting particles were collected by centrifugation and washed with acetone. The IZO QDs were dispersed in methanol. To further enhance the dispersion, ethanolamine ($HOCH_2CH_2NH_2$, Sigma-Aldrich) was added to the methanol dispersion at 0.5 vol% and mixed for 5 h with sonication (WUC-D10H, Wiseclean).

2.2. Fabrication of the drop-cast IZO QD layer

To compare the effect of morphology on the sensing performance, we prepared nonpatterned flat IZO QD layers by the drop-casting method. First, electrodes in the sensor devices were masked with tape, and only the IDE was exposed for drop casting. The devices were heated to 80 °C on a heating mantle for 5 min. Meanwhile, the synthesized IZO QD solution was sonicated for 5 min and drop cast on the IDE parts of the devices with syringes. After drying the IZO QD solution, the samples were heat treated at 600 °C for an hour in a tube furnace.

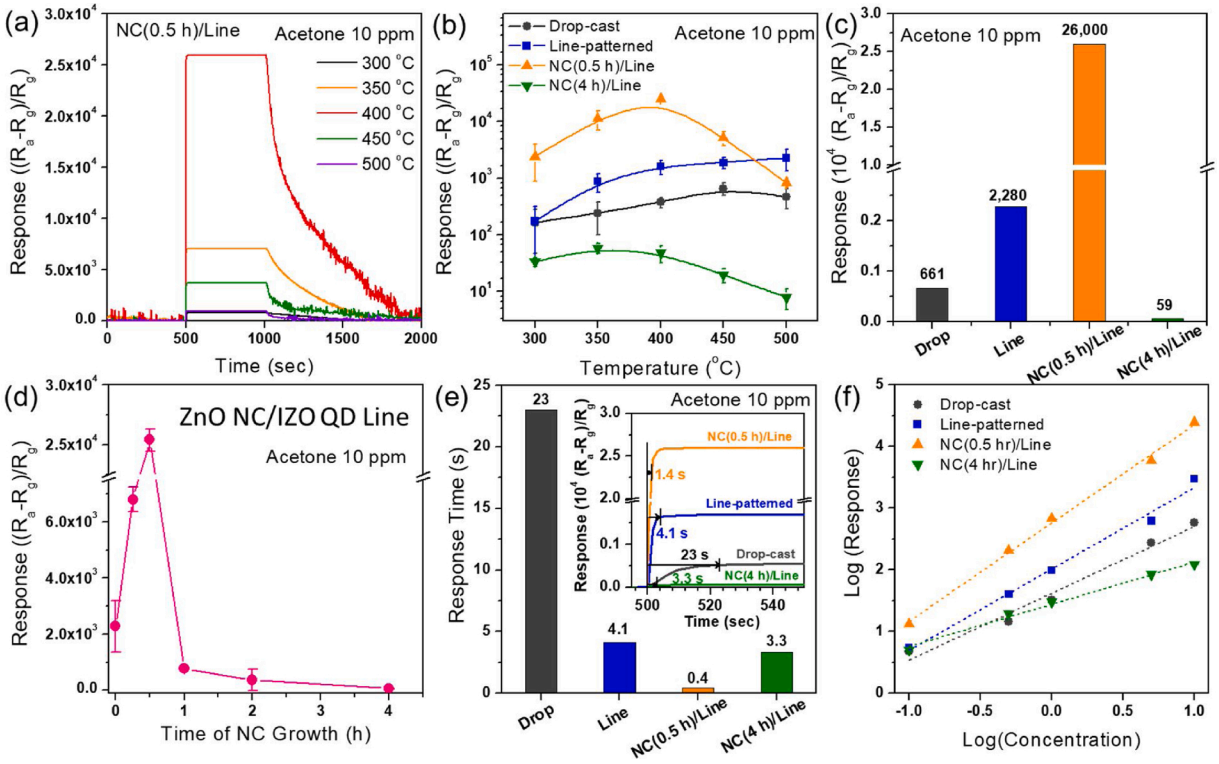

Fig. 4. (a) Sensing curves of NC (0.5 h)/line samples, (b) responses of drop-cast (black), line-patterned (blue), NC (0.5 h)/line (orange), and NC (4 h)/line (green) to 10 ppm of acetone at various temperatures (300 – 500 °C), and (c) optimal response of each sensor. (d) Responses of various samples with different time of hydrothermal growth to 10 ppm of acetone. (e) Response time of drop-cast (black), line-patterned (blue), NC (0.5 h)/line (orange), and NC (4 h)/line (green) samples to 10 ppm of acetone at their optimal temperatures, respectively. Inset depicts response times from their sensing curves. (f) Linear relationship between logarithms of response and concentration of acetone gas at optimized temperatures. (For interpretation of the references to colour in this figure legend, the reader is referred to the web version of this article).

2.3. Fabrication of the line-patterned IZO QD layer

2.3.1. Fabrication of a patterned PDMS stamp

A master mold was fabricated by photolithography (MJB6, SUSS MicroTec) using SU-8 as a negative photoresist. The pattern on the photomask has a periodic line/space with a height of 5 μm, and the linewidth and space are equal to 5 μm. The thickness of the photoresist was controlled to a value similar to the line width/space, allowing the aspect ratio of the pattern to be close to 1. Thus, the thickness of the photoresist was ~5 μm. An elastomeric polydimethylsiloxane (PDMS) stamp was replicated from the master mold prepared by photolithography. A 10:1 wt ratio of base resin and curing agent (Sylgard 184, Dow) was manually mixed and degassed in a desiccator for 1 h to drive out air bubbles trapped in the mixture during mixing. After pouring the mixture onto the master mold and curing the sample at 80 °C for 3 h, the cured and patterned PDMS stamp was peeled off from the master mold. Finally, the patterned PDMS stamp was cut to a small size (5×5 mm^2) for the following transfer molding step (see Fig. 1(a)).

2.3.2. Drop casting and transfer molding

Before the transfer molding of IZO QDs onto the IDE-patterned sensor substrate, the IZO QD dispersion in methanol and ethanolamine was first drop cast onto the cut PDMS stamp (5×5 mm^2) surface (see Fig. 1(b)). Specifically, 0.02 mL of the IZO QD dispersion was dropped and dried for 5 min in a desiccator; the same dropping/drying process was repeated four times for the transfer molding with a 5 μm line/space patterned PDMS stamp (for different pattern sizes or heights, the drop volume is different). Then, the sensor substrate with IDE was contacted with the drop-cast IZO QD/PDMS sample. Note that the boiling point of ethanolamine is very high (~170 °C), so the dried QD dispersion drops on the PDMS stamp are still in the liquid state. The drop-cast IZO QD/PDMS was contacted with the sensor substrate and was further left in under ambient conditions for 30 min to completely remove methanol from the dispersion drop. The assembly of (sensor substrate + drop-cast IZO QDs + PDMS stamp, from top to bottom) was placed on a hot plate maintained at 150 °C for 0.5 h. The assembly was then inverted (PDMS stamp + drop-cast IZO QDs + sensor substrate) and further heated at 150 °C for 2 h.

After this step, the QD layer solidified slightly, and the PDMS stamp was carefully removed from the sample (see Fig. 1(c)). The remaining sample, the patterned IZO layer on the IDE-patterned sensor substrate, was further annealed at 150 °C for 17 h. Then, the sample was slowly

Table 1
Comparison of acetone sensing performance of various gas sensors based on metal oxide semiconductors.

Material	T (°C)	Response	Concentration (ppm)	Sensitivity (ppm^{-1})	Detection limit (ppm)	Response time (s)	Reference
ZnO NC(0.5 h) /IZO QD Line	400	26,000	10	2600	0.1	< 1	This work
Pt-decorated Al-doped ZnO NPs	450	421	10	42.1	0.01	2.9	[7]
Pt-PS-WO_3 NFs	350	120.5	5	24.1	0.1	< 32	[16]
Pt-loaded SnO_2 NTs	350	93	5	18.4	1	> 120	[13]
Si-doped WO_3 NPs	400	4.5	0.6	7.5	0.02	> 780	[15]
Al-doped ZnO NPs	500	11.8	1	4.9	0.01	11	[9]

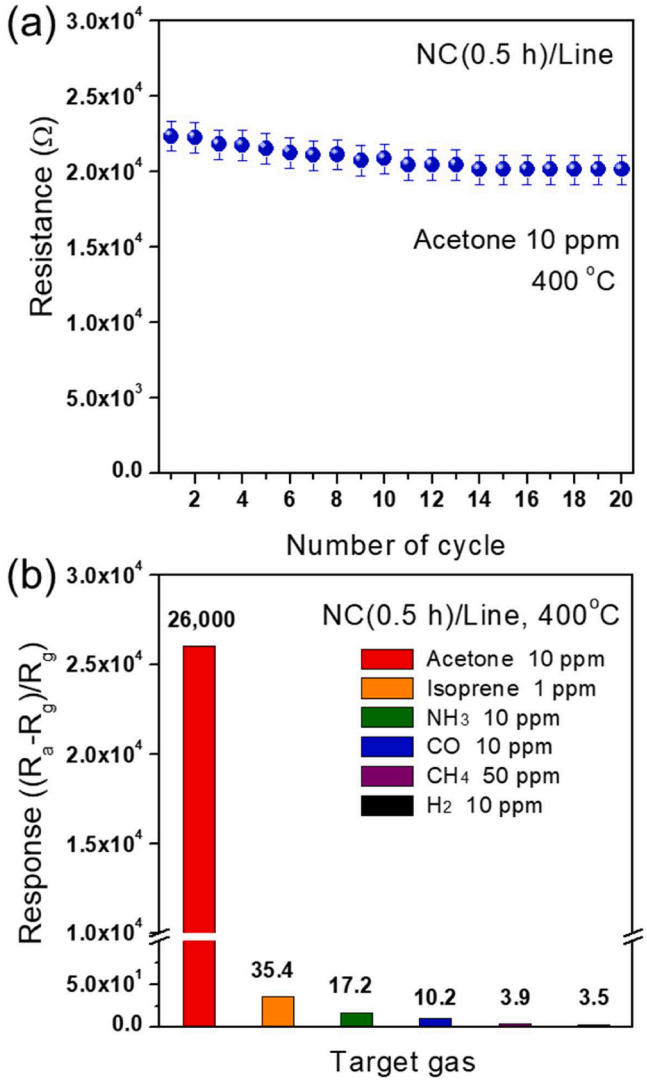

Fig. 5. (a) Repeatability test of NC (0.5 h)/line for 20 cycles at 400 °C. (b) Selectivity test of NC (0.5 h)/line for acetone (10 ppm), isoprene (1 ppm), NH_3 (10 ppm), CO (10 ppm), CH_4 (50 ppm) and H_2 (10 ppm) at 400 °C.

heated to 350 °C to completely remove the ethanolamine and to densify the patterned IZO QD layer. To leave only the line-patterned IZO QD layer on the IDE area of the sensor substrate, the 2×2 mm^2 area on the IDE was masked with tape, and the unmasked patterned IZO QD layer was etched away using Cr etchant (Sigma-Aldrich) (see Fig. 1(d)). A schematic of the final product of the line-patterned IZO QD layer is shown in Fig. 1(e).

2.4. Hydrothermal growth of ZnO nanocolumns

ZnO nanocolumns (NCs) were additionally grown on line-patterned IZO QD layers attached to the sensor substrate at 90 °C using a hydrothermal method. Aqueous solutions of zinc nitrate hexahydrate ($Zn(NO_3)_2{\cdot}6H_2O$, Sigma-Aldrich, 0.02 M) and hexamethylenetetramine (HMTA) ($(CH_2)_6N_4$, Sigma-Aldrich, 0.02 M) were used. For growth, all surfaces of the sensor devices except the area for growth on the IDE were masked with tape to prevent the electrodes from contacting the solution. The growth time varied at 0.5 h and 4 h. These samples were named NC (0.5 h)/Line (Fig. 1(f)) and NC(4 h)/Line (Fig. 1(g)), respectively.

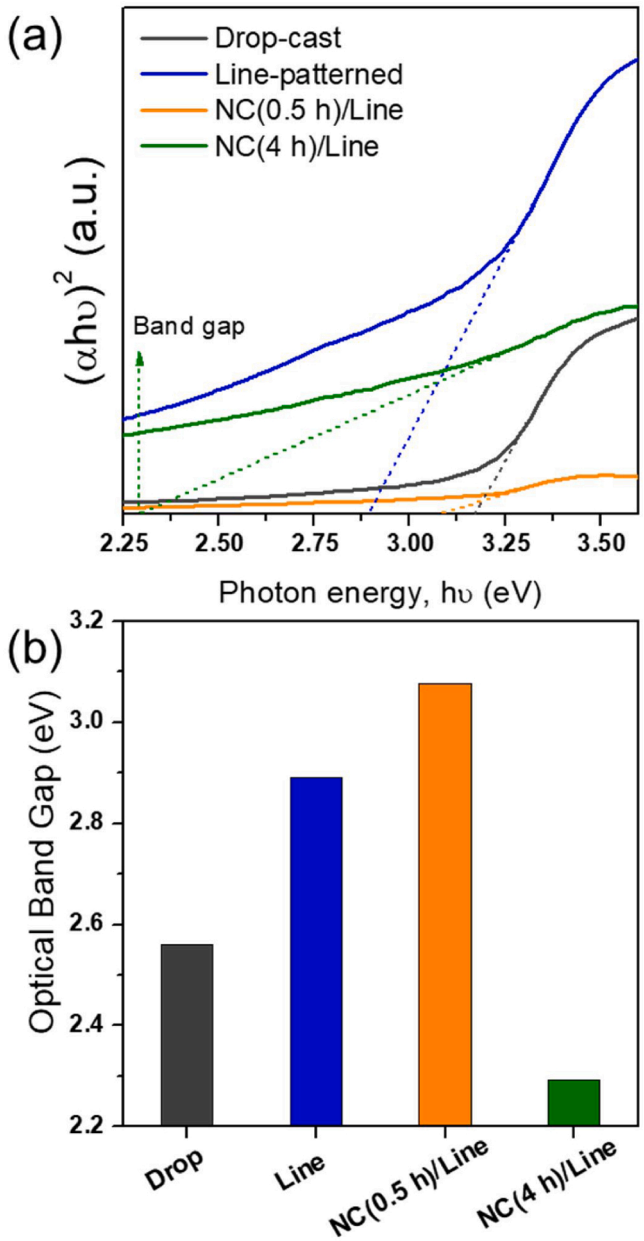

Fig. 6. (a) Calculated optical band energies of drop-cast (black), line-patterned (blue), NC (0.5 h)/line (orange), and NC (4 h)/line (green) sensors at room temperature. (b) The comparison of optical band gap energies. (For interpretation of the references to colour in this figure legend, the reader is referred to the web version of this article).

2.5. Characterization of sensing materials

The morphology of the sample surface was observed using scanning electron microscopy (SEM, S-5000 Hitachi). The crystal structures were measured by X-ray diffraction (XRD, SmartLab Rigaku) with Cu Kα radiation. The surface elements and their electronic states were investigated using XPS (K-alpha Thermo UK). The optical properties were measured using a UV–vis spectrophotometer (UV–vis, V-650, JASCO) in the wavelength range of 200–1200 nm.

2.6. Fabrication of the sensor device

To fabricate the sensor devices, Pt interdigitated electrodes (IDEs) were prepared on a SiO_2/Si substrate by photolithographic patterning,

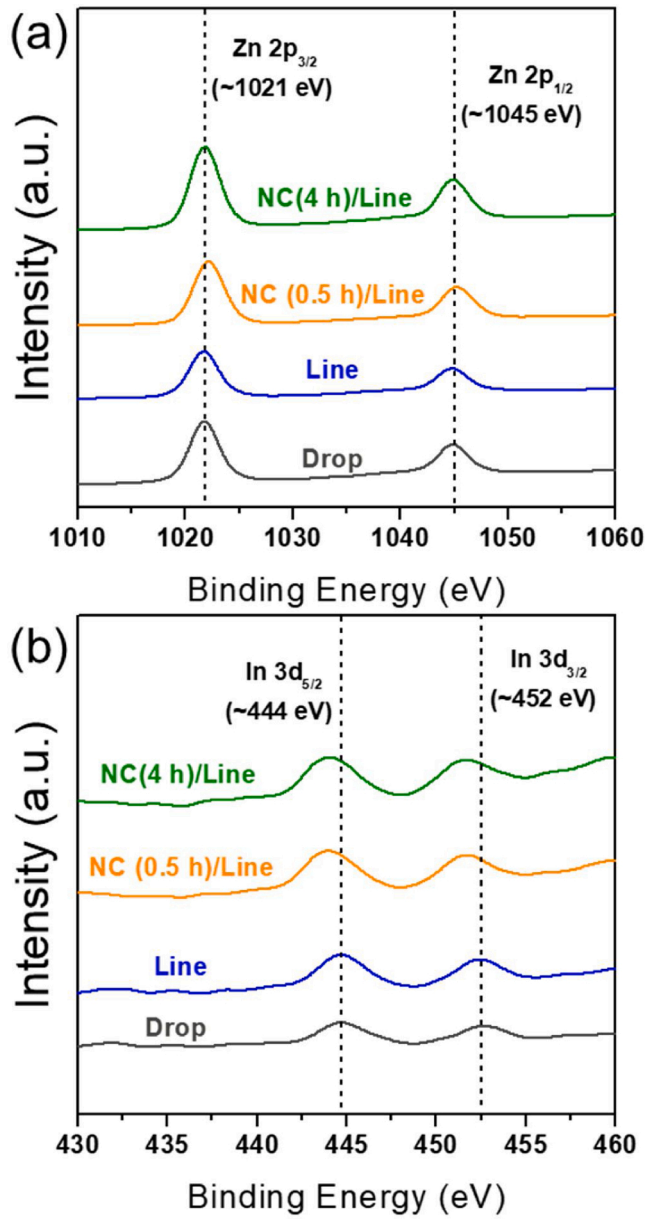

Fig. 7. (a) Zn $2p_{3/2}$ peaks and (b) In 3d peaks of drop-cast (black), line-patterned (blue), NC (0.5 h)/line (orange), and NC (4 h)/line (green) sensors from XPS at room temperature. (For interpretation of the references to colour in this figure legend, the reader is referred to the web version of this article).

Cr (20 nm)/Pt (100 nm) sputtering and lift-off processes. The Cr layer was used to provide good adhesion between the substrate and the Pt layer.

2.7. Gas sensing measurements

The fabricated sensor devices were tested with a customized sensor measurement system consisting of a tube furnace connected with mass flow controllers (MFCs). The concentration of acetone was controlled by mixing high concentrations of acetone with synthetic air gas. The sensing properties of the samples were tested by connecting Pt electrodes with a current source (Keithley 6220) with Pt wires and supplying a constant current of 10 nA at a time interval of 1 s. The resulting voltage was collected by a nanovoltmeter (Keithley 2182). All experiments were conducted at temperatures in the range of 300–500 °C. The response of a sensor (R) is described by the following equation:

$$R = \frac{R_a - R_g}{R_g} \quad (1)$$

where R_a and R_g represent the resistance of the sensor in air and in the target gas environment, respectively.

3. Results and discussion

To characterize the morphologies of the fabricated samples, we carried out SEM analysis. Fig. 2 shows the SEM images of the top and cross-sectional views of all prepared sensors. Fig. 2(a) shows the drop-cast IZO QD layer with a height of 500 nm. As shown in Fig. 2(b), the space between lines of the line-patterned IZO QD layer was approximately 5 μm. The cross-sectional area of the line has a trapezoidal shape with top, bottom, and height lengths of 1.8, 3.3 and 1 μm, respectively (see the inset of Fig. 2(b)). The trapezoidal shapes of the patterned lines are due to the shrinkage of the patterns upon the evaporation of ethanolamine. Fig. 2(c) and (d) show the successful growth of ZnO NCs on the IZO QD lines in the samples of ZnO NC(0.5 h)/IZO QD Line and ZnO NC(4 h)/IZO QD Line, respectively. In detail, ZnO NCs grown for 0.5 h have a diameter of ~ 170 nm and a height of ~ 500 nm (Fig. 2(c)). ZnO NC samples grown for 4 h exhibited thicker (300 nm in diameter) and longer (1 μm in height) NCs than those grown for 0.5 h (Fig. 2(d)) because of the longer growth time. In addition, the ZnO NC(4 h)/IZO QD Line sample exhibited a higher density of NCs than the sample grown for 0.5 h so that the line-patterned IZO QD layer was completely covered with the ZnO NCs.

Structural phase analysis of the prepared samples was conducted by XRD. Fig. 3 shows the XRD spectra of the drop-cast IZO QD layer, line-patterned IZO QD layer, ZnO NC(0.5 h)/IZO QD Line, and ZnO NC(4 h)/IZO QD Line. The XRD patterns of all samples exhibited diffraction peaks at 31.6, 34.4, 36.1, 47.4, 56.4, 62.6, 66.48, 67.9 and 69.19 of 2θ, which were assigned to (100), (002), (101), (102), (110), (103), (200), (112) and (201), respectively. The results indicate that all fabricated samples have polycrystalline hexagonal wurtzite structures of ZnO (JCPDS #36-1451). No characteristic peaks indicating impurities were detected.

The sensing properties of all fabricated sensors to 10 ppm acetone were investigated in a temperature range from 300 °C to 500 °C. Fig. 4 (a) shows the sensing response curves of the ZnO NC(0.5 h)/IZO QD Line to 10 ppm acetone at various operating temperatures. Those of all samples are shown in Figs. S1(a)-(d) of Supplementary material. The response curves were obtained from the change in sensing resistance at each operating temperature (Figs. S2(e)-(h)) according to the definition of response (Eq. (1)). As shown in Figs. S2(e)-(h), the initial resistance, which is the resistance of the sensor in air before exposure to acetone, decreases with increasing temperature. When the temperature of a semiconductor is increased, the density of the charge carriers increases, and consequently, the resistivity decreases. Therefore, the decrease in initial resistance is due to the intrinsic properties of semiconducting metal-oxide materials [21]. In addition, at the same operating temperature of 400 °C, the initial resistance of the samples in air decreased with the order of the drop-cast IZO QD layer, line-patterned IZO QD layer, ZnO NC(0.5 h)/IZO QD Line, and ZnO NC(4 h)/IZO QD Line samples (See Fig. S3). This is because more and more conduction paths are formed as more patterns and nano-columns are formed.

A comparison of the sensing responses for all sensors upon exposure to 10 ppm acetone is shown in Fig. 4(b), revealing the sensing responses as a function of operating temperatures. As shown in Fig. 4(c), the maximum responses of the drop-cast IZO QD layer, line-patterned IZO QD layer, ZnO NC(0.5 h)/IZO QD Line, and ZnO NC(4 h)/IZO QD Line samples are ~ 661 at 450 °C, ~ 2280 at 500 °C, ~ 26,000 at 400 °C, and ~ 59 at 350 °C, respectively. The results indicate that the line-patterned samples have significantly enhanced sensing responses compared to the regular drop-cast sample. In particular, as the surface structure of the sensors became more complicated by growing additional NCs, the

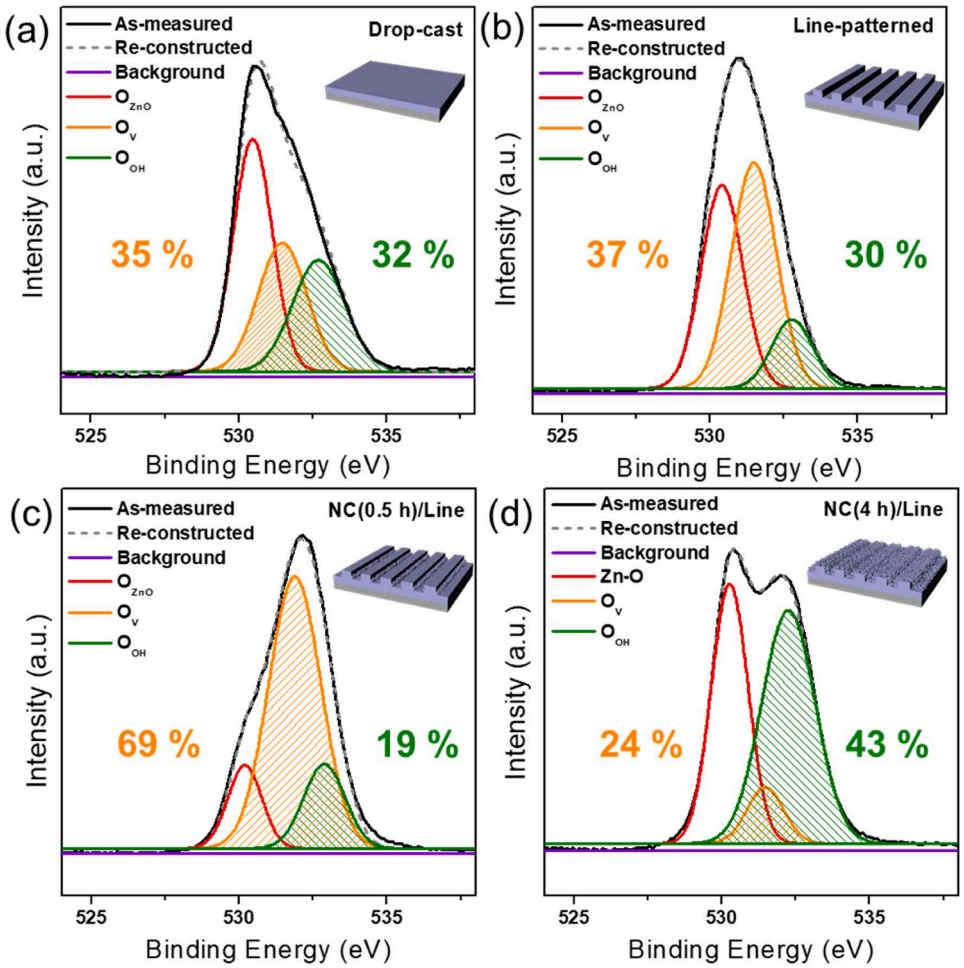

Fig. 8. O 1s peaks of (a) drop-cast, (b) line-patterned, (c) NC (0.5 h)/line, and (d) NC (4 h)/line sensors from XPS at room temperature. Orange and green numbers on each graph depict areal percentage of o-deficient and o-chemisorbed peaks, respectively. (For interpretation of the references to colour in this figure legend, the reader is referred to the web version of this article).

responses further increased (ZnO NC(0.5 h)/IZO QD Line). However, too much NC growth on the surface did not enhance their sensing properties but rather reduced them significantly (ZnO NC(4 h)/IZO QD Line).

Further, we found the optimal NC growth time for the best sensing response. Fig. 4(d) shows the responses of the ZnO NC/IZO QD Line samples with different times of NC growth (0, 0.25, 5, 1, 2, and 4 h) to 10 ppm acetone at their optimal working temperatures. Accordingly, the line-patterned IZO QD layer including ZnO NCs grown for 0.5 h showed the best sensing response (~ 26,000) to 10 ppm acetone at the optimal working temperature of 400 °C. These results implied the possibility that the optimal growth of NCs on the surface of the line-patterned sample could improve the sensing performance.

We determined the response time of the sensors to 10 ppm acetone by evaluating the time required to reach 90 % of the maximum response after exposure to the target gas, as seen in the inset of Fig. 4(e). Fig. 4(e) shows the response time of the drop-cast IZO QD layer, line-patterned IZO QD layer, ZnO NC(0.5 h)/IZO QD Line, and ZnO NC(4 h)/IZO QD Line samples to 10 ppm acetone at their optimal operating temperatures, with values of ~ 23, ~ 4.1, ~ 0.4, and ~ 3.3 s, respectively. As a result, we found that the response time for the line pattern-based samples was also significantly reduced compared to that of the drop-cast sample. The ZnO NC(0.5 h)/IZO QD Line sample has the shortest response time among all the samples.

In addition, we investigated the relationship between sensing responses and acetone concentrations for the prepared samples with different morphologies. The sensors were exposed to acetone at various concentrations in the range of 0.1–10 ppm at their optimal operating temperatures. The maximum sensing response of the samples as a function of acetone concentration is presented on a log scale in Fig. 4(f). All sensors were capable of detecting 0.1 ppm acetone. It was previously reported that the relationship between two variables can be explained by the equation below [22]:

$$\log[Response] = a\log[Concentration] + b, \quad (2)$$

where both a and b represent coefficients. When linear relations can be clearly achieved from all sensors, the slope represents the sensitivity of the sensor. The sensitivity of the sensors was evaluated as ~ 1.1, ~ 1.3, ~ 1.6, and ~ 0.7 for the drop-cast IZO QD layer, line-patterned IZO QD layer, ZnO NC(0.5 h)/IZO QD Line, and ZnO NC(4 h)/IZO QD Line, respectively. Among the samples, the ZnO NC(0.5 h)/IZO QD Line exhibited the highest sensitivity. Therefore, the ZnO NC(0.5 h)/IZO QD Line sensor was the best acetone sensor among all fabricated sensors.

We compared the acetone sensing performance of the ZnO NC (0.5 h)/IZO QD Line sensor with that of various previously reported gas sensors based on metal oxide semiconductors in Table 1. The sensitivity was estimated in terms of the ratio of the response to the acetone concentration. To our knowledge, our ZnO NC(0.5 h)/IZO QD Line sensor shows superior sensing performance both in terms of the sensitivity and response time.

To further verify the performance of the best sample as an acetone sensor, we tested the repeatability and selectivity of the ZnO NC(0.5 h)/IZO QD Line sample. For the repeatability test, the sensing responses

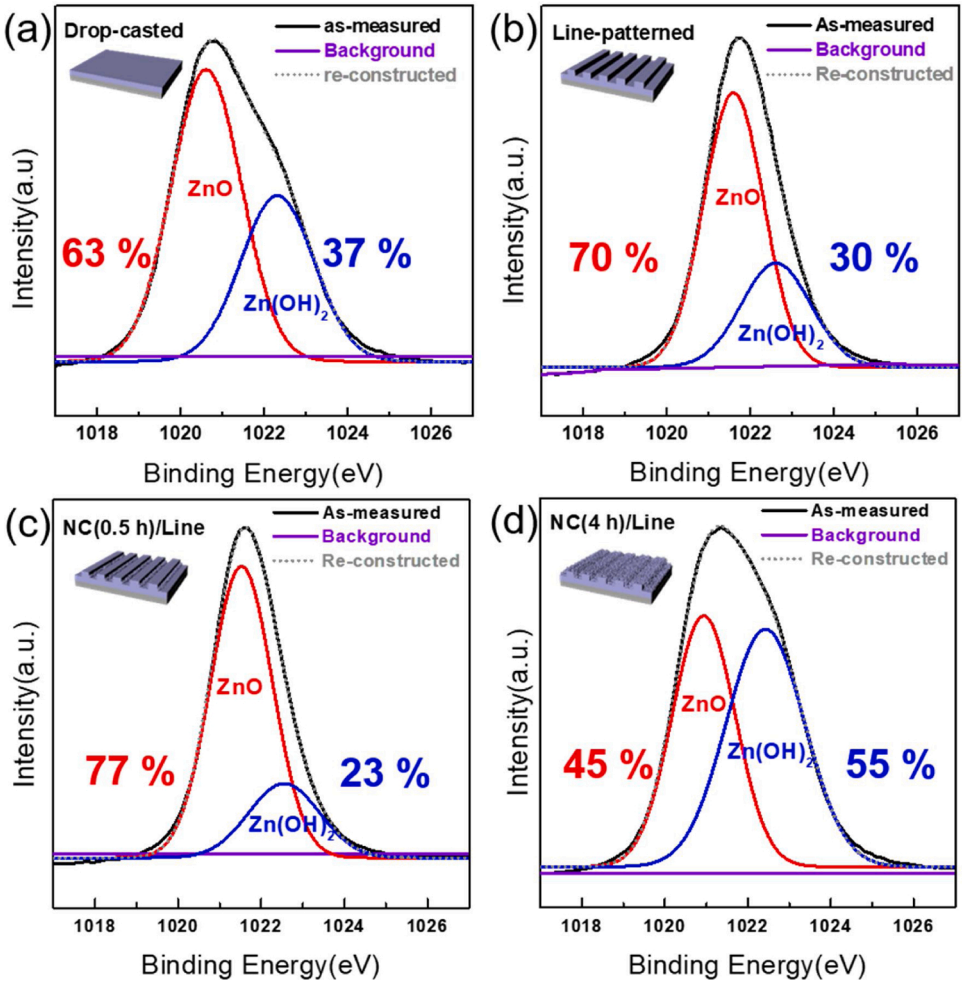

Fig. 9. Zn $2p_{3/2}$ peaks of (a) drop-cast, (b) line-patterned, (c) NC (0.5 h)/line, and (d) NC (4 h)/line sensors through XPS at room temperature. Red and blue numbers on each graph depict areal percentage of ZnO and $Zn(OH)_2$ peaks, respectively. (For interpretation of the references to colour in this figure legend, the reader is referred to the web version of this article).

were measured continuously with exposure to 10 ppm acetone at 400 °C for 20 cycles. The response was nearly constant without significant degradation (Fig. 5(a)). This result implies that the ZnO NC(0.5 h)/IZO QD Line sensor can be operated repeatedly for sensing 10 ppm acetone. Additionally, we examined the sensing performance of the ZnO NC (0.5 h)/IZO QD Line sensor to other gases to verify the selectivity for acetone. When the sample was exposed to various gases, such as 1 ppm isoprene, 10 ppm NH_3, 10 ppm CO, 50 ppm CH_4 and 10 ppm H_2, the response to other gases was less than 50, meaning that the ZnO NC (0.5 h)/IZO QD Line sensor shows a clear distinction when sensing acetone. Since the responses to any interfering gases were less than 1 % of the response to 10 ppm acetone, our sensors can selectively detect acetone.

To determine the relationship between electronic states and morphology in terms of its effect on the sensing properties of sensors, we performed UV–vis spectroscopy at room temperature. From UV–vis spectroscopy, the electronic structures of materials can be analyzed by evaluating optical band gaps. From the absorption spectra, the optical band energy (E_g) can be calculated by the Tauc equation [23,24]:

$$\alpha h\nu = C(h\nu - E_g)^n, \quad (3)$$

where α, hν, and C represent the absorption coefficient, energy of photons, and a constant, respectively. Additionally, n = 0.5 for semiconductors with direct band gaps. The optical band gap energy could be derived by extrapolating $(\alpha h\nu)^2$ to zero as a function of hν. The extrapolation lines and measured optical band energies are depicted in Fig. 6(a) and (b), respectively. The optical band energy of the drop-cast samples was approximately 2.56 eV, and it increased to 2.89 eV and 3.08 eV for the line-patterned and ZnO NC(0.5 h)/IZO QD Line samples, respectively. The ZnO NC(4 h)/IZO QD Line sample, on the other hand, exhibited a decreased optical band gap of 2.29 eV. The trend of the optical band energy of the samples (Fig. 6(b)) is in accordance with that of sensing responses (Fig. 4(c)). Generally, the optical band gap can be attributed to a change in the carrier concentration, which leads to a shift of the Fermi level inside the conduction band. Consequently, the optical band gap can be increased by increasing the carrier concentration of samples [8,24]. Therefore, the results indicate that the carrier concentrations increase from the drop-cast sample to the line-patterned and NC (0.5 h)/Line samples but decrease significantly for the NC(4 h)/Line sample. It was reported that the more oxygen vacancies exist, the higher is the carrier concentration and the electrical conductivity [25]. Therefore, the increased carrier concentration can be attributed to an increase in oxygen vacancies because electrons can be generated from the oxygen vacancies [24,25]. The comparison of the oxygen vacancy ratios of the prepared samples will be discussed using XPS analysis.

To understand the relationship between the oxidation states of the sample elements on the surface of the sensors and the morphology, which affects the sensing properties of the sensors, we conducted XPS at room temperature. First, the chemical state of the prepared sample surfaces was investigated by analyzing the Zn 2p and In 3d spectra, which are shown in Fig. 7(a) and (b), respectively. All samples exhibited

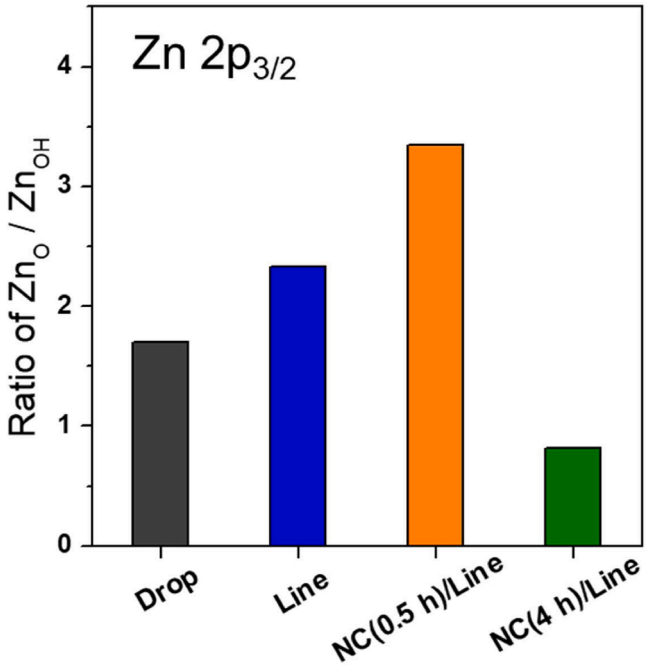

Fig. 10. Ratio between peaks areas of ZnO and $Zn(OH)_2$ peaks from Zn $2p_{3/2}$ peaks for drop-cast (black), line-patterned (blue), NC (0.5 h)/line (orange), and NC (4 h)/line (green) sensors at room temperature. (For interpretation of the references to colour in this figure legend, the reader is referred to the web version of this article).

two main peaks corresponding to the Zn $2p_{3/2}$ (~1021 eV) and Zn $2p_{1/2}$ (~1045 eV) states in Zn 2p spectra and the In $3d_{5/2}$ (~444 eV) and In $3d_{3/2}$ (~452 eV) states in In 3d spectra. The results of the Zn 2p and In 3d spectra indicate the presence of a divalent oxidation state in Zn–O bonding and an In dopant as In^{3+} at the Zn^{2+} sites of ZnO crystals in the samples, respectively. Furthermore, a peak shift to a lower binding energy was observed in the In 3d spectra only for NC(0.5 h)/Line and NC (4 h)/Line samples (Fig. 7(b)). In principle, the XPS peak shift can occur due to the charging effect on the sample surface or the surrounding [26]. Further study is needed to elucidate the reason for the peak shift.

We carried out a detailed analysis of the oxidation states of the samples by using XPS O 1s spectra. The O 1s peaks of the sensors are depicted in Fig. 8. The peaks were deconvoluted into three distinct Gaussian peaks centered at ~ 529.8, ~ 531.2, and ~532.5 eV [27]. The peak at ~ 529.8 eV (red line, O_{ZnO}) is attributed to O^{2-} from Zn–O bonds present in ZnO wurtzite. The peak at ~ 531.2 eV (orange line, O_V) is attributed to O- or O^{2-} ions in oxygen-deficient regions within the IZO and/or ZnO lattices and/or its surface imperfections [27]. The peak at ~ 532.5 eV (green line, O_{OH}) represents an absorbed hydroxyl group (—OH), which is formed preferably at the oxygen vacancy sites on the surface of the materials [28].

By comparing the ratio of peak areas, we could indirectly compare the ratio of oxygen ions in each electronic state. Among the three different types of oxygen ions, the O_V peak is known to be directly related to the performance of the sensors. For the drop-cast samples, the area of the O_V peak accounted for approximately 35 % of the total O 1s peak. The portion of the O_V peak gradually increased to 37 % and 69 % for the line-patterned and 0.5 h NC grown samples, respectively. This dramatic increase in oxygen vacancies can be attributed to an increase in the specific surface areas, which can produce more reactive sites for sensing. However, further growth of the NCs led to more adsorption of —OH groups from external sources rather than the creation of more vacancies ($O_V < O_{OH}$), as shown in Fig. 8(d). The increase in the portion of O_{OH} indicates a decrease in the number of reactive sites by covering the hydroxyl groups on the surface of the sensing materials.

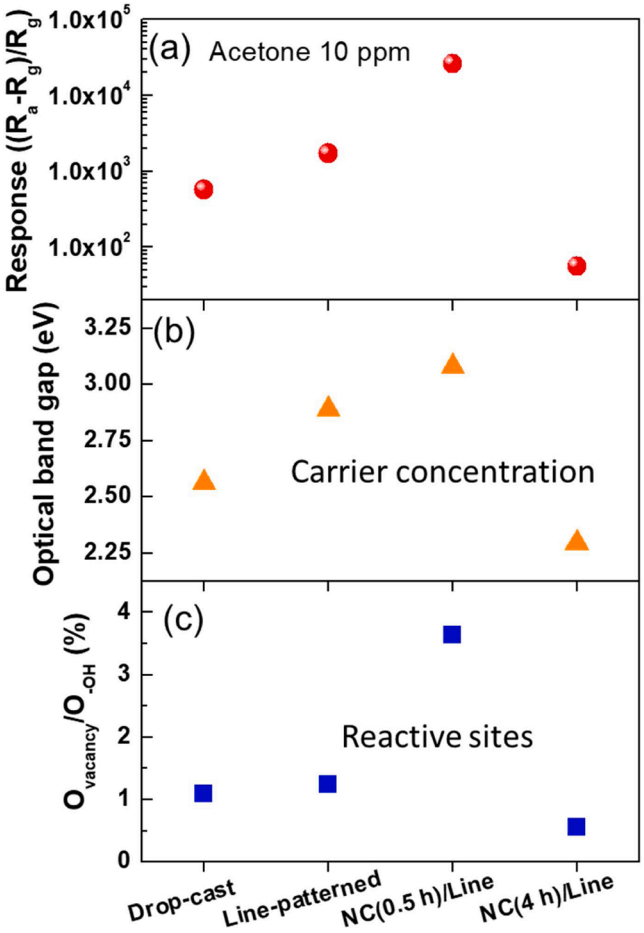

Fig. 11. Overall comparison of (a) responses, (b) optical band gap energies, (c) ratio between $O_{vacancy}$ and O_{-OH} for all sensors.

In addition, we analyzed the Zn $2p_{3/2}$ peaks in detail to compare the ratio of Zn-O (Zn_O) and Zn—OH (Zn_{OH}) bonds inside the lattices of different sensing materials. The Zn $2p_{3/2}$ peaks were deconvoluted into two separate Gaussian peaks at ~ 1022 eV (red) and ~ 1023.8 eV (blue), corresponding to ZnO and $Zn(OH)_2$, respectively (Fig. 9(a–d)) [29]. As shown in Fig. 9, the percentage of $Zn(OH)_2$ for the different samples exhibited a trend similar to that of the O_{OH} peaks in Fig. 8. This result suggests that the ZnO NCs are converted to $Zn(OH)_2$ during long-term growth. Therefore, the significant decrease in the carrier concentration for the NC(4 h)/Line sample can be explained by the increase in Zn $(OH)_2$ formation. The carrier concentration of ZnO composites has been reported to be closely related to the amount of $Zn(OH)_2$ formed [27]. As $Zn(OH)_2$ is converted to ZnO, the optical band gap energy increases, along with the concentration of carriers, such as oxygen vacancies. Since electrons are produced along with oxygen vacancies, materials with higher optical band gap energies may refer to those with higher concentrations of electrons as carriers. Therefore, we speculate that the ratio between ZnO and $Zn(OH)_2$ (Fig. 10) is responsible for the change in the carrier concentration (Fig. 6(b)).

An overall comparison of the introduced factors that affect the sensing responses is shown in Fig. 11. The increase in the optical band gap leads to an increase in the carrier concentration, which affects the improvement of the sensing performance (Fig. 11(b)). As previously reported, oxygen vacancies are considered to be active sites for the reaction between the surface of the sensing material and acetone molecules. The increase in the ratio of oxygen vacancies to hydroxyl groups indicates an increase in the effective amount of reactive sites against interfering sites by converting $Zn(OH)_2$ to ZnO structures (Fig. 11(c)).

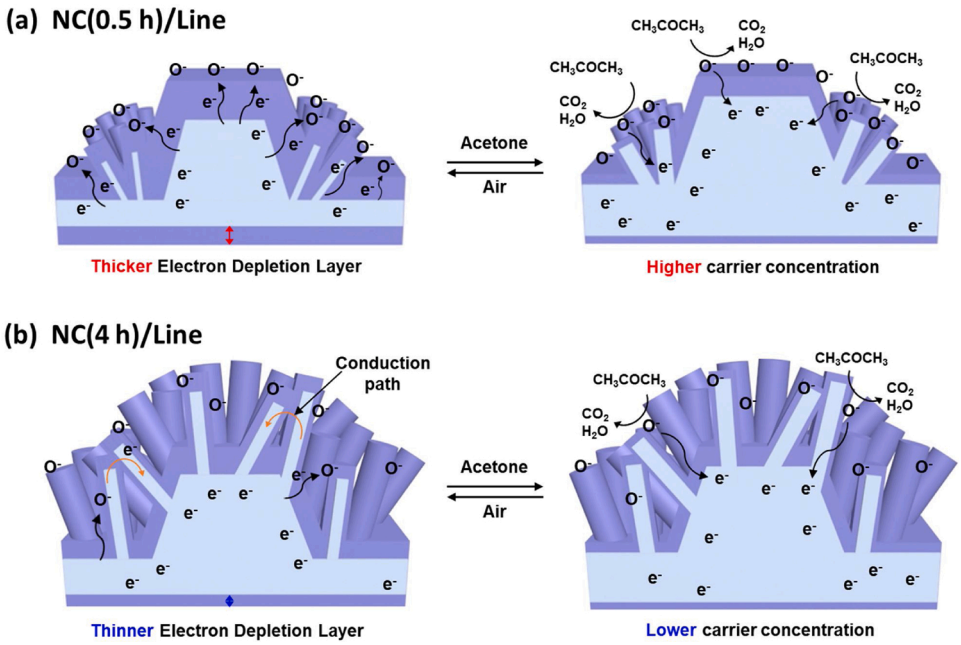

Fig. 12. Sensing mechanism of (a) NC (0.5 h)/line and (b) NC (4 h)/line sensors.

Therefore, the enhanced sensing responses from the drop-cast sample to the line-patterned and NC(0.5 h)/Line samples are attributed to the increased carrier concentration and active sites due to the increase in specific surface area. A large decrease in the response of NC(4 h)/Line may be caused by the significant decrease in the carrier concentration and active sites due to the formation of larger amounts of adsorbed hydroxyl groups and $Zn(OH)_2$.

Finally, based on these results, we propose a sensing mechanism for the NC(0.5 h)/Line and NC(4 h)/Line samples. The basic mechanism was based on the change in resistance under air and the target gas because of the thickness change in the electron depletion region [7,8,17]. Under ambient air conditions, electrons are transferred to the surface and react with oxygen molecules to produce oxygen species on the surface of sensing materials. As a consequence, thick electron depletion layers were formed on the surface of the sensors, thereby resulting in a high resistance of the sensors (Fig. 12(a), left). On the other hand, when sensors are exposed to target gases, the oxygen species act as functional groups and react with gas molecules. Subsequently, electrons released from the chemical reaction move back to the electron depletion region and decrease its thickness (Fig. 12(a), right). During this process, the resistance of gas sensors is also decreased, and the change in resistance is measured as a response. The XPS results revealed that during the long-term growth, many hydroxyl groups (—OH) are absorbed on the material surface (Fig. 8) and many ZnO NCs are converted to $Zn(OH)_2$ (Fig. 9). As a result, under air, the thickness of depletion regions in the NC(4 h)/Line sensors (Fig. 12(b), left) must be lower than that in the NC (0.5 h)/Line sensors (Fig. 12(a), left) because of the interference of —OH or $Zn(OH)_2$. Therefore, the change in the resistance and depletion layer thickness were less in the NC(4 h)/Line sensor than in the NC (0.5 h)/Line sensor. Thus, the response of the NC(4 h)/Line sensor is significantly reduced compared to that of the NC(0.5 h)/Line sensor.

4. Conclusion

We investigated the effect of the surface morphology of In-doped ZnO-based sensors on their sensing performances. ZnO-based sensors with various morphologies were prepared: a drop-cast IZO QD layer, a line-patterned IZO QD layer, and a line-patterned IZO QD layer with ZnO NCs grown for 0.5 h (NC(0.5 h)/Line) and 4 h (NC(4 h)/Line). Among the prepared samples, the NC(0.5 h)/Line sample exhibited an excellent sensing response of 26,000, a rapid response time of 0.4 s to 10 ppm of acetone and the highest sensitivity for various acetone concentrations. The NC(0.5 h)/Line sensor showed almost a constant resistance change after operating for 20 cycles and good selectivity for 10 ppm acetone over other interfering gases, such as isoprene, NH_3, CO, CH_4 and H_2. The superior sensing response of the NC(0.5 h)/Line sample to the drop-cast and line-patterned samples was explained by the large increase in the carrier concentration and active sites due to the increase in the specific surface area. The significantly decreased response of the NC(4 h)/Line sample was attributed to the large decrease in the carrier concentration and active sites due to the production of hydroxyl group bonds on the sensor surface and the formation of $Zn(OH)_2$ NCs instead of ZnO NCs. Accordingly, the results demonstrated that the fabrication of sensing materials with complicated surface nanostructures can dramatically enhance the sensing performance of sensors.

CRediT authorship contribution statement

Jun Ho Lee: Conceptualization, Investigation, Formal analysis, Validation, Writing - original draft. **Seung-Eun Baek:** Conceptualization, Investigation, Formal analysis, Validation. **Hyun-Sook Lee:** Conceptualization, Validation, Writing - original draft, Writing - review & editing. **Dahl-Young Khang:** Supervision. **Wooyoung Lee:** Supervision.

Declaration of Competing Interest

The authors report no declarations of interest.

Acknowledgements

This research was supported by the Basic Science Research Program (2017M3A9F1052297) and the Priority Research Centers Program (2019R1A6A1A11055660) funded by the National Research Foundation of Korea (NRF). This research was also supported by the Medium and Large Complex Technology Commercialization Project (2019K000045) of the Commercialization Promotion Agency for R&D Outcomes (COMPA) funded by the Ministry of Science and ICT (MSIT).

Appendix A. Supplementary data

Supplementary material related to this article can be found, in the online version, at doi:https://doi.org/10.1016/j.snb.2020.129131.

References

[1] M. Righettoni, A. Amann, S.E. Pratsinis, Breath analysis by nanostructured metal oxides as chemo-resistive gas sensors, Mater. Today 18 (2015) 163–171.
[2] T. Mathew, P. Pownraj, S. Abdulla, B. Pullithadathil, Technologies for clinical diagnosis using expired human breath analysis, Diagnostics 5 (2015) 27–60.
[3] Owlstone Medical.
[4] J. Pereira, P. Porto-Figueira, C. Cavaco, K. Taunk, S. Rapole, R. Dhakne, et al., Breath analysis as a potential and non-invasive frontier in disease diagnosis: an overview, Metabolites 5 (2015) 3–55.
[5] W. Miekisch, J.K. Schubert, G.F. Noeldge-Schomburg, Diagnostic potential of breath analysis—focus on volatile organic compounds, Clin. Chim. Acta 347 (2004) 25–39.
[6] H. Jung, W. Cho, R. Yoo, H.-s. Lee, Y.-S. Choe, J.Y. Jeon, et al., Highly selective real-time detection of breath acetone by using ZnO quantum dots with a miniaturized gas chromatographic column, Sens. Actuators B Chem. 274 (2018) 527–532.
[7] Y. Park, R. Yoo, S. Park, J.H. Lee, H. Jung, H.-S. Lee, W. Lee, Highly sensitive and selective isoprene sensing performance of ZnO quantum dots for a breath analyzer, Sens. Actuators B Chem. 290 (2019) 258–266.
[8] J.H. Lee, H. Jung, R. Yoo, Y. Park, H.-S. Lee, Y.-S. Choe, W. Lee, Real-time selective detection of 2-chloroethyl ethyl sulfide (2-CEES) using an Al-doped ZnO quantum dot sensor coupled with a packed column for gas chromatography, Sens. Actuators B Chem. 284 (2019) 444–450.
[9] M.S. Park, J.H. Lee, Y. Park, R. Yoo, S. Park, H. Jung, W. Kim, H.-S. Lee, W. Lee, Doping effects of ZnO quantum dots on the sensitive and selective detection of acetylene for dissolved-gas analysis applications of transformer oil, Sens. Actuators B Chem. 299 (2019) 126992.
[10] L. Liu, S. Li, J. Zhuang, L. Wang, J. Zhang, H. Li, et al., Improved selective acetone sensing properties of Co-doped ZnO nanofibers by electrospinning, Sens. Actuators B Chem. 155 (2011) 782–788.
[11] M.R. Alenezi, S.J. Henley, N.G. Emerson, S.R.P. Silva, From 1D and 2D ZnO nanostructures to 3D hierarchical structures with enhanced gas sensing properties, Nanoscale 6 (2014) 235–247.
[12] X. Kou, N. Xie, F. Chen, T. Wang, L. Guo, C. Wang, et al., Superior acetone gas sensor based on electrospun SnO2 nanofibers by Rh doping, Sens. Actuators B Chem. 256 (2018) 861–869.
[13] J.-S. Jang, S.-J. Kim, S.-J. Choi, N.-H. Kim, M. Hakim, A. Rothschild, et al., Thin-walled SnO 2 nanotubes functionalized with Pt and Au catalysts via the protein templating route and their selective detection of acetone and hydrogen sulfide molecules, Nanoscale 7 (2015) 16417–16426.
[14] S.-J. Choi, B.-H. Jang, S.-J. Lee, B.K. Min, A. Rothschild, I.-D. Kim, Selective detection of acetone and hydrogen sulfide for the diagnosis of diabetes and halitosis using SnO2 nanofibers functionalized with reduced graphene oxide nanosheets, ACS Appl. Mater. Interfaces 6 (2014) 2588–2597.
[15] M. Righettoni, A. Tricoli, S.E. Pratsinis, Si: WO3 sensors for highly selective detection of acetone for easy diagnosis of diabetes by breath analysis, Anal. Chem. 82 (2010) 3581–3587.
[16] S.-J. Choi, S.-J. Kim, W.-T. Koo, H.-J. Cho, I.-D. Kim, Catalyst-loaded porous WO 3 nanofibers using catalyst-decorated polystyrene colloid templates for detection of biomarker molecules, Chem. Commun. 51 (2015) 2609–2612.
[17] V.S. Bhati, M. Hojamberdiev, M. Kumar, Enhanced sensing performance of ZnO nanostructures-based gas sensors: a review, Energy Rep. 6 (2020) 46–62.
[18] B. Paul, B. Singh, S. Ghosh, A. Roy, A comparative study on electrical and optical properties of group III (Al, Ga, In) doped ZnO, Thin Solid Films 603 (2016) 21–28.
[19] Y. Xia, G.M. Whitesides, Soft lithography, Annu. Rev. Mater. Sci. 28 (1998) 153–184.
[20] M.A. Unger, H.-P. Chou, T. Thorsen, A. Scherer, S.R. Quake, Monolithic microfabricated valves and pumps by multilayer soft lithography, Science 288 (2000) 113–116.
[21] R. Yoo, A.T. Güntner, Y. Park, H.J. Rim, H.-S. Lee, W. Lee, Sensing of acetone by Al-doped ZnO, Sens. Actuators B Chem. 283 (2019) 107–115.
[22] N. Hongsith, E. Wongrat, T. Kerdcharoen, S. Choopun, Sensor response formula for sensor based on ZnO nanostructures, Sens. Actuators B Chem. 144 (2010) 67–72.
[23] P.K. Baviskar, P.R. Nikam, S.S. Gargote, A. Ennaoui, B.R. Sankapal, Controlled synthesis of ZnO nanostructures with assorted morphologies via simple solution chemistry, J. Alloys Compd. 551 (2013) 233–242.
[24] C.E. Kim, P. Moon, S. Kim, J.-M. Myoung, H.W. Jang, J. Bang, et al., Effect of carrier concentration on optical bandgap shift in ZnO: Ga thin films, Thin Solid Films 518 (2010) 6304–6307.
[25] G.J. Fang, D.J. Li, B.L. Yao, Effect of vacuum annealing on the properties of transparent conductive AZO thin films prepared by DC magnetron sputtering, Physica Status Solidi A Appl. Res. 193 (2002) 139.
[26] S. Tardio, P.J. Cumpson, Practical estimation of XPS binding energies using widely available quantum chemistry software, Surf. Interface Anal. 50 (2018) 5–12.
[27] S.Y. Park, J.H. Song, C.-K. Lee, B.G. Son, C.-K. Lee, H.J. Kim, et al., Improvement in photo-bias stability of high-mobility indium zinc oxide thin-film transistors by oxygen high-pressure annealing, IEEE Electron Device Lett. 34 (2013) 894–896.
[28] S. Dhara, K. Imakita, P. Giri, M. Mizuhata, M. Fujii, Aluminum doped core-shell ZnO/ZnS nanowires: doping and shell layer induced modification on structural and photoluminescence properties, J. Appl. Phys. 114 (2013), 134307.
[29] J. Ferreira, K. Souza, J. Rossi, I. Costa, J. Trindade, C. Tomachuk, Corrosion protection of electrogalvanized steel by surface treatments containing cerium and niobium compounds, Int. J. Electrochem. Sci. 11 (2016) 6655–6672.

Jun Ho Lee received a Bachelor's degree and a Master's degree in Material Science and Engineering at Seoul National University in 2015 and 2017, respectively. Since 2017, he has been working on developing a miniaturized GC that is integrated with a metal oxide-based gas sensor as a researcher at Yonsei University.

Seung-Eun Baek received a Bachelor's degree in Polymer Engineering at Gyeongsang National University in 2018. Since 2018, she is working on Development of patterned and selectively grown metal oxide nanorods based gas sensors as her Master's degree at Yonsei University.

Hyun-Sook Lee received a Ph.D. degree in Physics at POSTECH in 2008. Since 2015, she has been working as a research professor in the Department of Materials Science and Engineering at Yonsei University. Her research interests are in various materials related to high-temperature superconductors, solid-state hydrogen storages, rare-earth/rare-earth-free permanent magnets, and nanostructured metal oxide semiconductor gas sensors.

Dahl-Young Khang received his B.S. (1994), M.S. (1996), and Ph.D. (2000), all in Chemical Engineering, from the Seoul National University (SNU) under the supervision of Prof. Hong H. Lee. His Ph.D. work was on the nanoscale and unconventional patterning using nanoimprint lithography. After working for a start-up company for years, which is set up to adapt the unconventional patterning techniques to various fields such as optical elements in liquid crystal display, he joined the Prof. John A. Rogers' group at the University of Illinois at Urbana-Champaign (UIUC) as a post-doctoral research fellow in 2003. His research at UIUC was on the high performance flexible and/or stretchable electronics using thin films of single-crystalline semiconductor elements such as Si. In 2008, he joined the Department of Materials Science and Engineering, Yonsei University. His current research is focused on soft electronics, which includes electronic, photovoltaic, and optoelectronic devices using organic/inorganic active materials on bendable or stretchable substrates.

Wooyoung Lee is the Dean of School of Materials Science and Engineering and the Director of Institute of Nanoscience and Nanotechnology at Yonsei University in Korea. He received a BS degree in Metallurgical Engineering in 1986, a MS degree in Metallurgical Engineering from the Yonsei University in 1988. He received a Ph.D. degree in Physics from University of Cambridge, United Kingdom in 2000. He is a regular member of National Academy of Engineering of Korea. He was a member of National Science & Technology Council and a director in Korea Israel Industrial R&D Foundation. In recent years, his research interests have centered on hydrogen sensors, various metal oxide semiconducting gas sensors, and breath analyzers. He is also studying thermoelectric materials and devices, and permanent magnets. He has received a number of awards in nano-related research areas and a Service Merit Medal (2008) from the Government of Korea due to contribution on the development of intellectual properties. He has authored and co-authored over 200 publications, and has edited three special books on nano-structured materials and devices.